CCFE-PR(15)55

M. J. Fleming, L. W. G. Morgan, and E. Schwageraus

Optimisation Algorithms for Multi-Group Energy Structures

Optimisation Algorithms for Multi-Group Energy Structures

M. J. Fleming [a,b], L. W. G. Morgan [a], E. Schwageraus [b]

[a]CCFE, Culham Science Centre, Abingdon, Oxon, OX14 3DB, United Kingdom
[b]Department of Engineering, University of Cambridge, Trumpington Street, Cambridge CB2 1PZ, United Kingdom

Optimisation Algorithms for Multi-Group Energy Structures

M. J. Fleming[a,b,*], L. W. G. Morgan[a], E. Schwageraus[b]

[a] *CCFE, Culham Science Centre, Abingdon, Oxon, OX14 3DB, United Kingdom*
[b] *Department of Engineering, University of Cambridge, Trumpington Street, Cambridge CB2 1PZ, United Kingdom*

Abstract

Modelling of nuclide densities as a function of time within magnetic confinement fusion devices such as the JET, ITER and proposed DEMO tokamaks is performed using Monte-Carlo transport codes coupled with a Bateman equation solver. The generation of reaction rates occurs either through point-wise interpolation of energy dependent tracked particle data with nuclear data or multi-group convolution of 'binned' fluxes with binned cross-sections. The multi-group approach benefits from decreased computational expense, but introduces errors through effects such as self-shielding. Depending on the multi-group structure and nuclear data used, this method can introduce unacceptable errors without warning. We present a multi-group optimisation method which utilises a modified particle swarm algorithm followed by a non-stochastic 'string-tightening' algorithm. This procedure has been used with a semi-homogenised 1D DEMO-like reactor design in order to produce an optimised energy group structure for tritium breeding. In this example, the errors introduced by the Vitamin-J 175 multi-group are reduced by two orders-of-magnitude in the optimised group structure.

Keywords: Fusion neutronics, Monte-Carlo, Multi-group, MCNP, Reaction rate, ITER, DEMO

1. Introduction

One of the great benefits of Monte-Carlo (MC) particle transport codes such as MCNP [1] lies in the fact that phase space does not need to be specifically discretised. MC codes take advantage of the full, continuous energy data – although at the cost of execution time and local nature of outputs, such as flux tallies. While point-wise (PW) calculations enjoy greater accuracy, multi-group (MG) methods are still of fundamental importance due to computational resource limits and data portability. MC calculations using PW convolutions (for example, the `FM` multipliers of MCNP) must refer to and interpolate within nuclear data for each reaction – in addition to running the transport calculations. When using energy bin multipliers (as provided by another code or the `EM` multipliers of MCNP), the user specifies the cross-section for a set of bins and MCNP will simply tally the population in each bin before taking the convolution of histograms. This benefits from a significant decrease in the computational expense when compared with PW convolution. While a 'point-wise flux' is effectively calculated through the set of all particles which are tallied, this data cannot be used by other software, such as inventory codes. MG fluxes and effective cross-sections can be easily used as inputs for other codes which can perform whatever user-specific tasks which are not within the capabilities of MCNP[1].

As a simplified integral method MG convolution can only provide approximate values of reaction rates, but it also suffers from systematic errors due to numerous factors such as self-shielding, which is temperature and material composition specific. Multiple methodologies exist to address this concern, but a brute-force alternative would be to use a large number of bins (such as the 43000 bin default of VESTA for fission applications [2]). A recent study found that several thousand groups would be necessary to meet desired accuracy for fusion applications, when bins were chosen as equal lethargy [3], although fewer would be required with self-shielding corrections.

We present an optimisation for MG energy group structure which we use to limit MG deviations from PW calculation. It has been demonstrated that the Vitamin-J 175 group structure[2] overestimates total tritium-producing effective cross-sections [6]. To demonstrate the capabilities of this optimisation, it has been employed to decrease the MG error in the tritium-yielding reactions which occur in the blanket modules of a simplified DEMO-like reactor. The optimisation performed in this study can easily be applied to other reactor designs or sets of reactions relevant for other systems.

2. Optimisation Methods

With a goal of minimising the point-wise to multi-group (PW-MG) deviation, we have chosen to take the

*Corresponding author
Email address: `michael.fleming@ccfe.ac.uk` (M. J. Fleming)

[1] Such as multi-phase irradiation pulses which cannot be accurately handled by CINDER - a common issue for fusion analysis.

[2] Whose raison d'être is fusion neutronics and shielding [4, 5].

sum of square deviations over all bins as our fitness function. We will employ a meta-heuristic algorithm based on the Particle Swarm Optimisation (PSO) approach to minimise the function. Due to the fact that algorithms of this class cannot locate global optima in general, and that the number of iterations we will be able to complete is much less than would be required to perform a fine search of the space of multi-groups[3], we will follow the modified PSO with a non-stochastic 'string-tightening' algorithm to fine-tune the multi-group structure.

To optimise on a multi-dimensional space with a fitness function which takes the time required for an MCNP simulation (with individual bin variance much less than PW-MG deviation) and has numerous deep minima, we employ a meta-heuristic, stochastic algorithm which uses swarm intelligence [7]. This concept requires multiple test solutions to be tracked simultaneously, so that collective knowledge can be implicitly created through the sharing of information between the multiple members of the 'swarm'. As one of a variety of swarm-based optimisations that have seen wide use, particle swarm optimisation [8] benefits from being a simple core concept that is easy to implement and easily modified in a surprising number of ways for adaptation to problem-specific features.

The collection of particles in our swarm will represent different multi-group energy structures, *ie* vectors of 174 energies in sequence for a Vitamin-J 175 group example. During each iteration, the algorithm generates group-wise evaluated nuclear data files (GENDFs) for each reaction and for each PSO particle. These are used to automatically generate MCNP inputs which will be executed to calculate MG and PW reaction rates over each bin for each swarm particle. The square of the PW-MG deviation in each bin is summed to provide a fitness value for each swarm particle, or energy group. Each of the 174-dimensional positions are updated by swarm-guided motion before the new multi-groups are used in the next iteration. For each particle i there exists a unique energy group for each iteration, whose j energies $x_{i,j}$ yield individual bin fitness values,

$$f_{i,j} \equiv f(x_{i,j}) = \left[\left(\int_{x_{j-1}}^{x_j} \sigma(x)\phi(x)dx \right) - \sigma_j \phi_j \right]^2 , \quad (1)$$

where the integral indicates PW convolution and the simple product MG convolution. The units in all deviations-per-bin figures are (barns/source neutron)^2. The particle fitness, $f_i = \sum_j f_{i,j}$, is used by the PSO algorithm to update energy group structures using a random walk coupled with pulls toward personal, local and/or global best positions. We follow the standard PSO implementation where in each iteration the positions are moved with an updated velocity $v_{i,j}$ based upon the best personal MG for each individual particle $p_{i,j}$ and the global best energy group $g_{i,j}$:

$$\begin{aligned} x_{i,j}[t+1] &= x_{i,j}[t] + v_{i,j}[t] & (2) \\ v_{i,j}[t+1] &= v_{i,j}[t]I[t] + c_1[t]r_1\left(p_{i,j} - x_{i,j}[t]\right) & (3) \\ &\quad + c_2[t]r_2\left(g_{i,j} - x_{i,j}[t]\right). \end{aligned}$$

The 'inertia' $I[t]$, personal preference $c_1[t]$ and global preference $c_2[t]$ parameters are varied over the course of the optimisation, along with the random numbers r_1, r_2. We will take this 'fully informed' PSO approach, where every particle is drawn toward the global best position as well as its own best. In addition to this position motion, we add a 'teleport' modification which removes each particle's bin with the best fitness $\{x_{i,b}|f_{i,b} < f_{i,j\neq b}\}$ and adds a position near the worst energy bin $\{x_{i,w}|f_{i,w} > f_{i,j\neq w}\}$. This can be controlled with a threshold parameter (*ie* only if $f_{i,b} < kf_{i,w}$, for some k) to speed up migration of energy groups over large energy ranges.

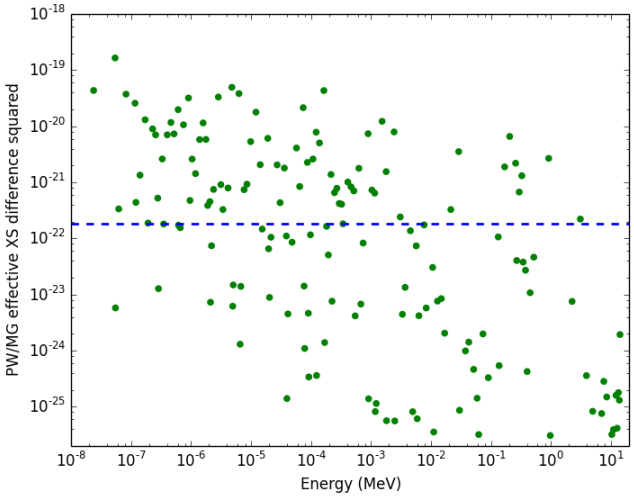

Figure 1: Particle swarm output multi-group square deviations example against the deviation per bin for the 'ideal' 175 group solution in blue.

While PSO can probe a large subset of the parameter space, it cannot identify a specific pattern such as equal lethargy. The output of a PSO run should still have large variance over bin fitness, as seen in Figure 1. The goal of a MG optimisation will be the minimisation of the differences in PW-MG deviations over all bins, into what we will refer to as the 'ideal' MG. While this energy structure and the constant PW-MG deviation is not known *a priori*, we include the average of the final output from section 4 in Figure 1. The PSO MG output is then used as the seed for a non-stochastic 'string tightening' algorithm. This algorithm still employs stochastic transport simulations, but we simulate enough particles to keep the transport variance well below the magnitude of the PW-MG deviations.

[3]In two optimisation runs using 20-particle swarms, approximately 12000 MCNP simulations were carried out with sufficient particles for PW-MG deviations *in each bin* to be significantly greater than the relative error.

The position updates are given by the velocities[4]:

$$v_j = T\,(x_j - x_{j-1})\left(\frac{f_{j+1} - f_j}{f_{j+1} + f_j}\right) \quad \text{if } f_j > f_{j+1} \quad (4)$$

$$v_j = T\,(x_{j+1} - x_j)\left(\frac{f_{j+1} - f_j}{f_{j+1} + f_j}\right) \quad \text{if } f_j < f_{j+1}. \quad (5)$$

The 'tension' parameter T determines how far each bin can be pulled/pushed by a neighbour and must be less than 0.5 – if $T = 0.5$ and $f_{i+1}[t] \gg f_i[t]$, then we can obtain overlapping bins $f_{j-1}[t+1] = f_j[t+1]$. The energy groups are effectively represented as a series of connected string sections with tension proportional to the difference between neighbouring errors. Bins with larger errors pull the nearby group boundaries toward their energy, leading to migration of bin density toward regions with greater overall error. As shown in Figure 2, the algorithm minimises local deviations in PW-MG error, followed by migration of energy bin density through error 'waves'.

As the PW-MG deviations decrease, the statistical variation of the transport calculation becomes increasingly important and the stochastic nature of the fitness function will generate fluctuations which prevent the optimisation from progressing. Additionally, threshold reactions will cause large fluctuations where bins jump between either containing the reaction or not.

3. Software

Nuclear data processing is performed by the NJOY processing system [9], a FORTRAN-90 code which calls modules sequentially to produce and modify data for specific applications. For our purposes the following modules are used:

- `RECONR` – Reconstructs the resonances and produces PENDF data
- `BROADR` – Adds temperature-dependent Doppler broadening of resonances
- `UNRESR` – Produces 'effective self-shielded' cross-sections, using average value resonance data from ENDF
- `THERMR` – Generates neutron scattering cross-sections for (temperature-specific) thermal energies
- `ACER` – Prepares ACE format libraries for use by MCNP
- `GROUPR` – Creates multi-group data with multiple subroutines designed to counter possible error introduction, including the Bondarenko narrow-resonance

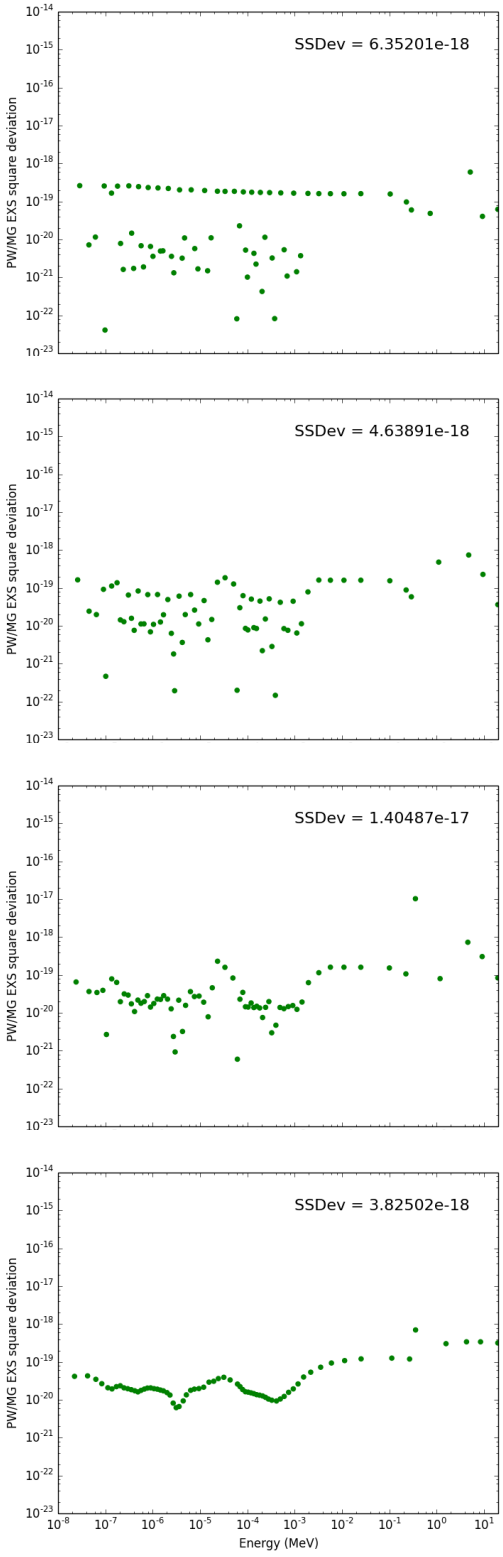

Figure 2: Example of evolution over non-stochastic algorithm with 69-group energy structure. Iterations 0, 1, 2 and 10 are shown.

[4] *nb* Our convention was to take f_j to sum the group immediately below energy x_j, and there is only one energy group being tested in each iteration, so we omit the particle index.

scheme [10] and user-specified weighting flux[5]

The optimisation procedure that was implemented utilised the point-wise convolution capabilities of MCNP which will call upon the ACE files. We therefore must use PENDF files processed in the same manner (and from the same raw source) to create ACE and GENDF data, as shown in Figure 3. All NJOY modules except `GROUPR` are called before the optimisation algorithm loop to produce PENDF and ACE files, while the optimisation will make repeated use of `GROUPR` to produce new GENDFs in each iteration.

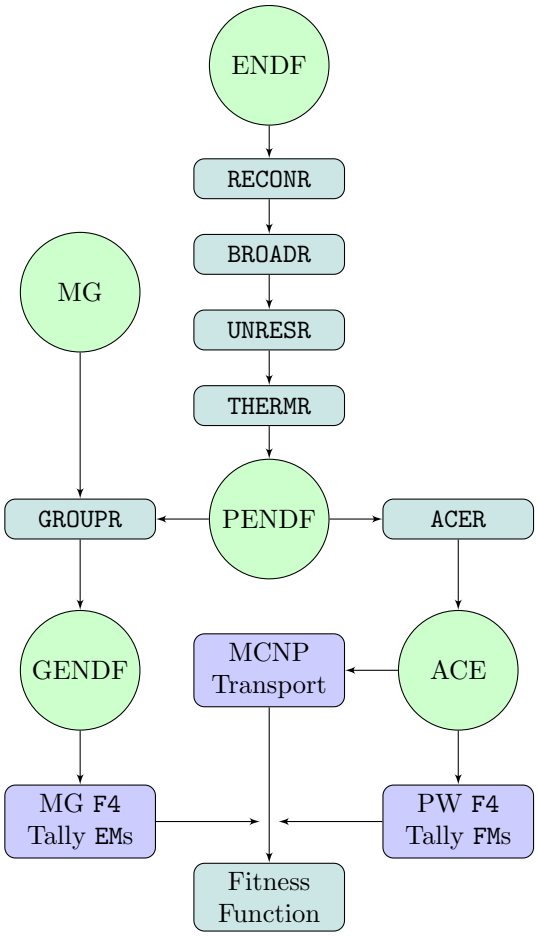

Figure 3: Flowchart of NJOY module execution and use of outputs.

The `F4` tallies of MCNP use `EM` energy multipliers with two sets of data: MG energy bin-cutoffs with arbitrary MG constants. We take the cross-sections from GENDF files to generate MG convolved reaction rates. The tally can also use `FM` tallies which interpolate within the PW ACE files. Comparing these for each bin, as in equation (1), generates our fitness function.

[5]This methodology allows the calculation of multiple dilution-specific cross-sections to correct for self-shielding. Additionally, multiple-dilution group data can be processed by `MATXSR` for use with codes such as TRANSX [11]. We avoid these issues with our choice of reactions in this paper and use infinitely dilute data with the `iwt=8` 'fusion peak' weighting of NJOY.

Throughout the optimisation we ensured that the variance in each bin remains significantly less than the PW-MG deviation for the algorithm to continue improving the MG structure. This requires vastly different parameters depending on the materials, design and MG bin density. With sets of reactions that contain multiple resonances and thresholds the MG structure will be very sensitive to small modifications, while high bin density will require exorbitant simulation time to obtain good individual bin statistics. We generally allow large uncertainties in early iterations and increase the number of particles simulated (`nps`) to around 1E8 in the final iterations.

4. Tritium Breeding Blanket Test Case

We modelled a ceramic lithium orthosilicate pebble blanket with a low pressure helium purge gas[6]. This was layered with beryllium slabs which were separated by Eurofer sheets and high pressure helium coolant channels. The remaining structural materials was a mixture of Eurofer and Inconel-718 steels and magnets made of niobium-tin, as will be used in ITER. These are the materials used in many DEMO studies and their nuclide fractions are summarised in Table A.2 of Appendix A.

The optimisation was performed on a spherical reactor with concentric shells of homogenised material. Each of the blanket layers contained the same mixture and radial variation of the flux was dealt with by splitting the 60cm blanket into four 15cm sections. A geometric cross-section of the reactor is presented in Figure 4 and the material composition of each of the cells is given, with the specific boundary radii, in Table 1.

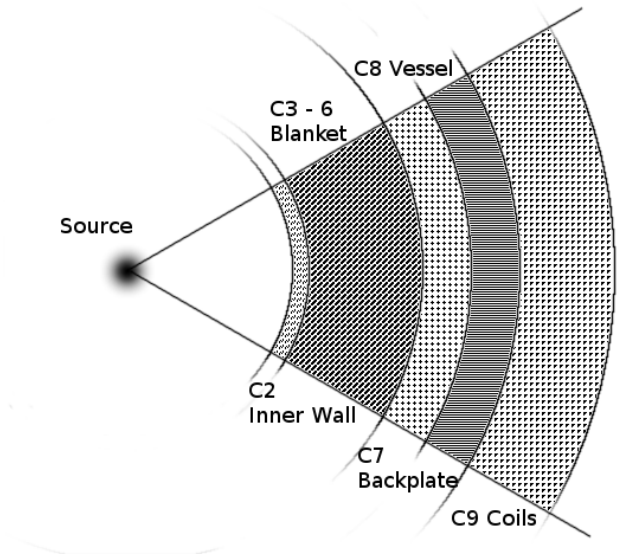

Figure 4: Geometric cross-section of the tritium breeding sphere model with homogenised blankets (not to scale).

[6]Based on one of the EU breeder module designs [12].

Table 1: Cellular break-down of tritium breeding reactor model with homogenised blanket layers by % volume.

Cell(s)	Outer Radii (cm)	Material Composition
1	1000	Void
2	1005	First wall
3,4,5,6	1020,1035,1050,1065	55% Be, 10% Eurofer, 20% He, 15% $LiSO_4$
7	1105	80% Eurofer, 20% He
8	1145	80% Inconel-718, 20% He
9	1365	70% NbSn Coil, 20% He 10% Inconel-718

The ^{6}Li, ^{7}Li and ^{9}Be are responsible for virtually all tritium production within proposed blanket modules for fusion reactors and their total (n,Xt) cross-sections are shown in Figure 5. Note that this set of reactions contains no narrow resonances and the total reaction rate for tritium production will be dominated by lower-energy ^{6}Li reactions. For our fitness function we have used the sum over all square PW-MG deviations of each tritium-producing reaction:

$$f_{i,j} = f_{i,j}(^6\text{Li}) + f_{i,j}(^7\text{Li}) + f_{i,j}(^9\text{Be}). \qquad (6)$$

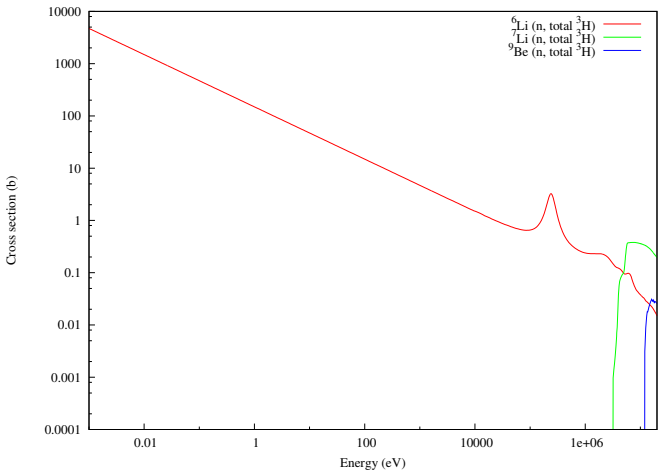

Figure 5: Point-wise cross-sections for total tritium production reactions within the breeding blanket.

For PSO the choice of seed solutions are, due to the stochastic nature of the optimisation and limited number of algorithm iterations possible, of tremendous importance. The balance we must reach rests between selecting seeds which are close enough to the ideal solution in order to limit execution time while being distant enough to probe a large subset of the space of multi-groups. The modified particle swarm algorithm was run with 20 seed particles, each of which contain three groups of equal lethargy bins, so that N energies between E_1 and E_2 are given by

$$E_i = E_1 \exp\left\{\frac{i}{N}\log\left(\frac{E_2}{E_1}\right)\right\} \quad i = 0, \ldots, N. \qquad (7)$$

N_T (themal) energies were chosen between 10^{-2} and 1 eV, N_I (intermediate) between 1 and 10^6 eV and N_F (fast) between 1 and 19.64 MeV, with a variety chosen for different seeds. The initial seed values for particles $j = 0, 1, \ldots, 19$ were taken as

$$N_{T_j} = 5 + j \; N_{I_j} = 115 - \left\lfloor \frac{j}{2} \right\rfloor \; N_{F_j} = 55 - \left\lceil \frac{j}{2} \right\rceil,$$

with floor and ceiling functions, respectively. After 145 iterations, the global best sum of squared deviations was reduced by nearly four orders of magnitude, from the Vitamin-J value of 4.84×10^{-15} to 7.31×10^{-19}. A second run was carried out with modified initial conditions. Seeds in the second optimisation were constructed in the same manner as the first, but the three-region bin numbers were based off of the results of the first run, where the global best energy group structure contained 38 energies below 1 eV, 125 between 1 eV and 1 MeV and 13 above 1 MeV. The second set of seeds were then taken as

$$N_{T_j} = 33 + \left\lceil \frac{j}{2} \right\rceil \; N_{I_j} = 127 - \left\lfloor \frac{j+1}{4} \right\rfloor \; N_{F_j} = 16 - \left\lfloor \frac{j+3}{4} \right\rfloor.$$

This second optimisation resulted in a global best energy group with a similar 6.95×10^{-19} sum of square deviations over a 145 iteration run. Both are summarised in Figure 6.

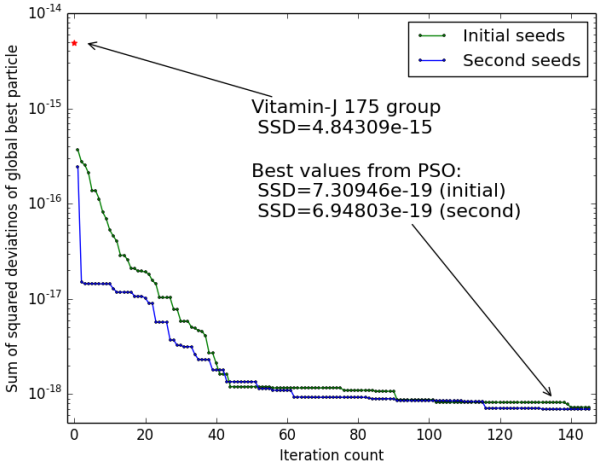

Figure 6: Global best sum of squared PW/MG deviations over PSO runs.

The resulting best energy group from the PSO was used as the input for the non-stochastic algorithm, which was run over 250 iterations with increasing `nps` and decreasing tension, from 5E5 to 1E7 and 0.2 to 0.05, respectively. The square PW-MG deviation in each bin is summarised in Figure 7.

The sum of square PW-MG deviations was reduced through this optimisation by over 5 orders of magnitude, producing a MG structure which contains a much higher

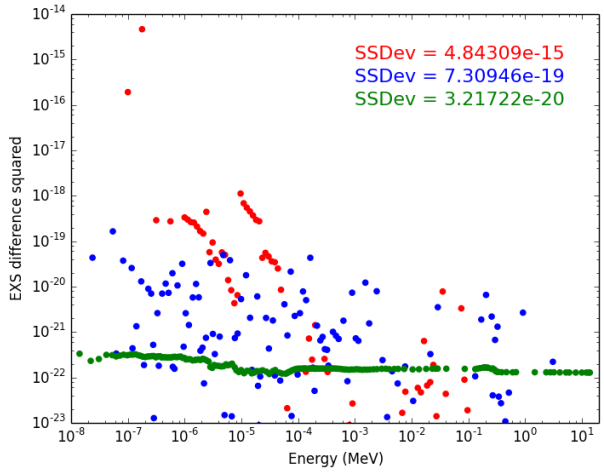

Figure 7: Square PW/MG deviations over the 175 group PSO and non-stochastic optimisation. Red shows the Vitamin-J structure, blue the PSO output and green the final energy group.

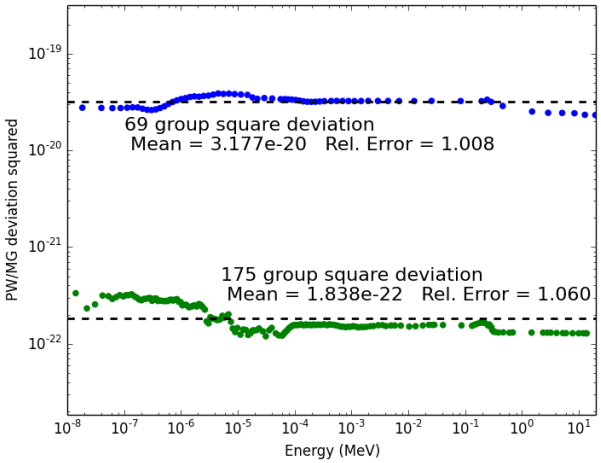

Figure 8: Square deviations for each bin in final energy groups against corresponding mean square deviations.

thermal-energy bin density. The total (n,Xt) deviation in the reaction rate has dropped from the Vitamin-J value of 1.2%, to a PSO output deviation of 0.03% and a final optimised deviation which is less than 0.01%. At this point the MG error can no longer be discerned from the statistical uncertainties of the MC simulation.

An optimisation was run with a 69 bin MG[7] with a hand-made non-stochastic seed MG extracted from the 175 output. With considerably fewer groups the MCNP simulation requirements for low-uncertainty calculations were considerably relaxed and the optimisation produced a MG with 0.03% PW-MG reaction rate deviation. The final MG square deviations are shown in Figure 8 against the final 175 MG output. A comparison of the relative number of bins per energy 'decade' is shown in Figure 9. The mean square deviations $\bar{f} = \frac{1}{n}\sum_{i=1}^{n} f_i$ both represent bin-error distributions which have similarly converged, with similar relative errors $var(f_i)/\bar{f} \approx 1$. With more than double the bin density, the 175-group structure possesses less than 1% the $\bar{f}$ of the 69-group. While the total reaction rate deviation does not reflect this difference, due to counteracting under/over-estimations, the substantially lower square deviation of the finer group makes it a more robust MG, less susceptible to increased errors with modifications in geometry, materials and/or flux.

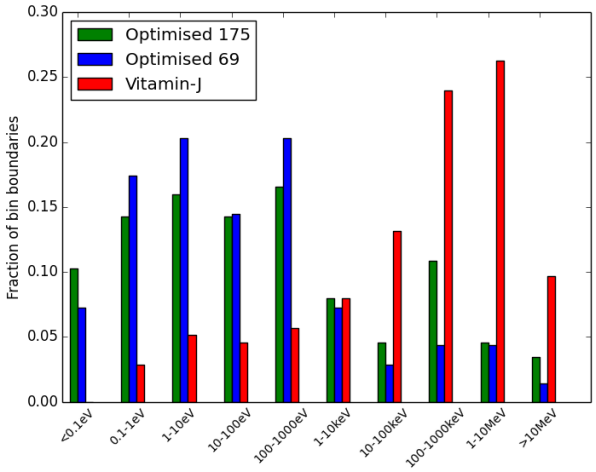

Figure 9: Distribution of energy bins by decade for the 69 optimised structure compared with the optimised 175 and Vitamin-J multi-groups.

5. Discussion

Note that the distributions in Figure 9 do not agree completely, particularly with the region around the 244 keV resonance of ^{6}Li(n,α)^{3}H. This generally reflects the lack of convergence upon our 'ideal' equal deviation-per-bin MG. Due to the fact that the total deviations are too small (with respect to the MC statistical uncertainty) to optimise, we cannot find the ideal and there exists a space of MG energy structures which all possess less PW-MG deviation than can be determined from MCNP calculations with reasonable simulation time. By decreasing the number of bins we can enter a regime where an optimal MG theoretically could be determined.

Working with fewer MG bins generally makes the optimisation much easier to perform. To give an illustration, see Figure 10 with the TRIPOLI-315 MG and the result of 200 iterations of the non-stochastic algorithm which has ordered the deviations into a string but has not decreased the variation in bin error. In this simple formulation, the algorithm is not appropriate for migrating bins, especially

[7]Chosen for EASY-II [13] compatability reasons in future work. Note that the WIMS-69 MG does not extend to 14 MeV and cannot be used for D-T fusion analysis.

where deviations are already so small. The TRIPOLI case provides a more pronounced example of what occurs when attempting to use the string algorithm with Vitamin-J as an initial MG, although in both cases the string algorithm fails to improve a MG structure with many bins and large regions with substantially different PW-MG errors. This underlines the purpose of the PSO; to find a more suitable seed for the string optimisation which was found to be inefficient in those circumstances. Any alternative process for obtaining such a seed MG would suffice and *in this simple model* such a MG could be obtained by intuitive guesswork. Most cases of interest will include many more nuclides and reactions, making the task of finding such a seed profoundly more challenging. The PSO we have applied is not meant to demonstrate an efficient method for this problem, but rather the capability of the method to be applied to similar (but more complex) problems. Since PSO depends only upon the fitness function and not the intricacies of the nuclear data, it can be utilised for other applications such as shielding and activation MG optimisation.

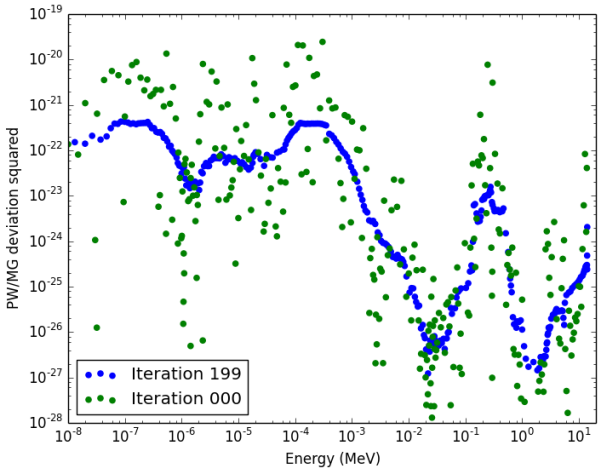

Figure 10: Evolution of TRIPOLI 315 multi-group square deviations over 200 iterations of the non-stochastic optimisation.

We have purposefully chosen an example with no narrow resonances and which has relatively little MG-PW error in general. An optimisation with many reactions will certainly possess considerably greater deviations and nearly every application will involve reactions with non-trivial resonances. Self-shielding corrections are implemented ubiquitously and a specific methodology must be chosen, which the optimisation must incorporate. A natural extension of this work would be to use an inventory code such as FISPACT-II [14] to collapse the spectrum with probability table corrections, or an alternative MC transport code which can accept repeated data modification and incorporate MG self-shielding corrections.

6. Summary

An optimisation methodology using PSO with a 'string-tightening' algorithm for minimising deviations between point-wise (PW) and multi-group (MG) convolution has been presented. The algorithms used a combination of NJOY processing and MCNP tallies to calculate reaction rates and took total squared PW-MG deviation over each bin to generate a fitness function. The optimisation can be applied to other systems and reaction sets with the introduction of self-shielding corrections, where necessary.

Optimisation of two MG structures was performed on a simplified concentric sphere model of a magnetic confined fusion reactor. Total tritium production through reactions with ^{6}Li, ^{7}Li and ^{9}Be were used to generate the fitness function. In this simple case, the Vitamin-J structure introduced a 1.2% error *solely* due to the MG convolution. The Vitamin-J group structure is far too coarse in the low-energy range, as it was not designed for representation of neutron spectra for thermal reactions. After optimisation the error was taken down to the statistical uncertainty of the transport simulation. Optimisation for a 69-bin MG resulted in a 0.03% total reaction rate error, while the TRIPOLI 315 MG deviation was at the transport uncertainty without modification. The errors that the Vitamin-J MG introduce can easily be avoided by using an energy structure optimised for an application or a finer MG, such as the TRIPOLI 315 or CCFE 709.

Acknowledgements

Thanks are due to J-Ch. Sublet for guidance and comments, as well as D. Kotlyar for suggestions early in the work. This research has received funding from the RCUK Energy Programme [grant number EP/I501045].

Appendix A. Reference Data

For reference, we include the atomic fractions of the materials which were used in the material specification for the tritium breeding concentric sphere model in Table A.2. The cells are those described in Table 1 and Figure 4. Note that the blanket (cells 3-6) is a homogenised material including the Eurofer steel, beryllium and lithium ceramic, as well as the helium purge and coolant gas. In Table A.3 we list the optimised energy groups with the original Vitamin-J multi-group given for comparison.

References

[1] J. F. Briesmeister, MCNP - A General Monte Carlo N-Particle Transport Code, Version 4C, Los Alamos National Laboratory, USA, LA-UR-05-8225 (December 2000).

[2] W. Haeck, E. Létang, Y. Calzavara, S. Fuard, Generic monte carlo depletion with VESTA, Transactions of The American Nuclear Society 99 (2008) 657–658.

Table A.2: Simplified DEMO-like model atom fractions by cell and densities in g/cm^3.

	Cell 2	Cells 3-6	Cell 7	Cell 8	Cell 9
Density	7.528	2.131	6.296	6.577	6.313
^{3}He	2.10019E-11	7.48667E-11	9.97068E-11	1.00395E-10	1.02771E-10
^{4}He	1.50014E-05	5.34762E-05	7.12191E-05	7.17109E-05	7.34075E-05
^{6}Li		5.50544E-03			
^{7}Li		6.79004E-02			
^{9}Be		7.36907E-01			
^{12}C	5.20676E-03	5.15578E-04	5.49313E-03		
^{13}C	5.84437E-05	5.78715E-06	6.16582E-05		
^{14}N	1.68695E-03	1.67043E-04	1.77973E-03		
^{15}N	6.19691E-06	6.13623E-07	6.53774E-06		
^{16}O	3.29352E-04	7.70772E-02	3.47466E-04		
^{17}O	1.25455E-07	2.93598E-05	1.32355E-07		
^{50}Cr	4.16488E-03	4.09970E-04	4.36796E-03	9.18855E-03	7.43317E-03
^{52}Cr	8.11668E-02	7.98965E-03	8.51244E-02	1.79070E-01	1.44860E-01
^{53}Cr	9.20149E-03	9.05748E-04	9.65014E-03	2.03003E-02	1.64221E-02
^{54}Cr	2.32459E-03	2.28821E-04	2.43793E-03	5.12850E-03	4.14874E-03
^{55}Mn	5.75567E-03	5.69931E-04	6.07223E-03		
^{54}Fe	4.82666E-02	4.77940E-03	5.09213E-02	1.09324E-02	3.41673E-02
^{56}Fe	7.63944E-01	7.56464E-02	8.05961E-01	1.73034E-01	5.40786E-01
^{57}Fe	1.74758E-02	1.73047E-03	1.84370E-02	3.95829E-03	1.23709E-02
^{58}Fe	2.49655E-03	2.47210E-04	2.63386E-03	5.65470E-04	1.76727E-03
^{58}Ni				3.73181E-01	1.17162E-01
^{60}Ni				1.43573E-01	4.50756E-02
^{61}Ni				6.02789E-03	1.89249E-03
^{62}Ni				1.97276E-02	6.19359E-03
^{64}Ni				5.47990E-03	1.72044E-03
^{63}Cu	3.56780E-02				2.00289E-02
^{65}Cu	1.58798E-02				8.91461E-03
^{90}Zr	2.80384E-05				
^{91}Zr	6.09768E-06				
^{92}Zr	9.30985E-06				
^{94}Zr	9.47318E-06				
^{96}Zr	1.52442E-06				
^{93}Nb				3.14727E-02	2.71051E-02
^{92}Mo				2.70666E-03	3.46338E-04
^{94}Mo				1.70081E-03	2.17631E-04
^{95}Mo				2.90784E-03	3.72079E-04
^{96}Mo				3.05414E-03	3.90800E-04
^{97}Mo				1.75567E-03	2.24651E-04
^{98}Mo				4.40747E-03	5.63969E-04
^{100}Mo				1.75567E-03	2.24651E-04
^{112}Sn					7.61289E-05
^{114}Sn					5.05014E-05
^{115}Sn					2.86426E-05
^{116}Sn					1.10048E-03
^{117}Sn					5.84158E-04
^{118}Sn					1.83840E-03
^{119}Sn					6.48227E-04
^{120}Sn					2.44216E-03
^{122}Sn					3.43711E-04
^{124}Sn					4.25116E-04
^{181}W	2.62124E-04	2.59557E-05	2.76541E-04		
^{182}W	9.04794E-04	8.95935E-05	9.54558E-04		
^{183}W	4.92522E-04	4.87700E-05	5.19611E-04		
^{184}W	1.05737E-03	1.04702E-04	1.11553E-03		
^{186}W	9.85044E-04	9.75399E-05	1.03922E-03		

[3] L. Morgan, J.-C. Sublet, W. Haeck, J. Pasley, Optimising the energy group structure used for fusion systems, Annals of Nuclear Energy 55 (2013) 108 – 115. doi:http://dx.doi.org/10.1016/j.anucene.2012.11.028.

[4] E. Sartori, Vitamin-j, a 175 group neutron cross section library based on jef-1 for shielding benchmark calculations, Tech. Rep. JEF/DOC-100, NEA Data Bank (October 1985).

[5] P. Vontobel, S. Pelloni, JEF/EFF Based Nuclear Data Libraries, Tech. Rep. EIR-Report 636, Paul Scherrer Institute (December 1987).

[6] A. Aures, L. Packer, S. Zheng, Tritium self-sufficiency of HCPB blanket modules for DEMO considering time-varying neutron flux spectra and material compositions, Fusion Engineering and Design 88 (9-10) (2013) 2436–2439. doi:10.1016/j.fusengdes.2013.05.042.

[7] G. Beni, J. Wang, Swarm intelligence in cellular robotic systems, Proceedings of NATO Advanced Workshop on Robots and Biological Systems.

[8] J. Kennedy, R. Eberhart, Particle swarm optimization, Proceedings of IEEE International Conference on Neural Networks 4 (1995) 1942 – 1948.

[9] R. E. MacFarlane, A. Kahler, The NJOY Nuclear Data Processing System, Version 2012, Los Alamos National Laboratory, LA-UR-12-27079 (December 2012).

[10] I. Bondarenko, Group Constants for Nuclear Reactor Calculations, Consultants Bureau, 1964.

[11] R. E. MacFarlane, TRANSX 2: A Code for Interfacing MATXS Cross-Section Libraries to Nuclear Transport Codes, Los Alamos National Laboratory, LA-12312-MS (July 1992).

[12] L. Giancarli, M. Abdou, D. Campbell, V. Chuyanov, M. Ahn, M. Enoeda, C. Pan, Y. Poitevin, E. Rajendra Kumar, I. Ricapito, Y. Strebkov, S. Suzuki, P. Wong, M. Zmitko, Overview of the ITER TBM Program, Fusion Engineering and Design 87 (5-6) (2012) 395–402. doi:10.1016/j.fusengdes.2011.11.005.

[13] J.-C. Sublet, J. Eastwood, G. Morgan, A. Koning, D. Rochman, EASY-II: a system for modelling of n, d, p, γ and α activation and transmutation processes, Joint International Conference on Supercomputing in Nuclear Applications and Monte Carlodoi:http://dx.doi.org/10.1051/snamc/201402103.

[14] J.-Ch. Sublet, J. W. Eastwood, J. G. Morgan, The FISPACT-II User Manual, Tech. Rep. CCFE-R(11) 11 Issue 6, CCFE (2014).

Table A.3: Summary of final 175 and 69 bin optimised energy group structures in eV with Vitamin-J included as a reference.

Bin	Vitamin-J	Opt. 175	Opt. 69	Bin	Vitamin-J	Opt. 175
0	1.0000E-05	1.0000E-05	1.0000E-05	88	2.8725E+05	8.5059E+01
1	1.0000E-01	4.2698E-03	1.8432E-02	89	2.8725E+05	8.5059E+01
2	4.1399E-01	9.9754E-03	3.9887E-02	90	2.9452E+05	9.0384E+01
3	5.3158E-01	1.6160E-02	6.2406E-02	91	2.9720E+05	9.6065E+01
4	6.8256E-01	2.3099E-02	8.6862E-02	92	2.9850E+05	1.0188E+02
5	8.7642E-01	3.2352E-02	1.1327E-01	93	3.0197E+05	1.0840E+02
6	1.1254E+00	4.2161E-02	1.4125E-01	94	3.3373E+05	1.1471E+02
7	1.4450E+00	5.2218E-02	1.7345E-01	95	3.6883E+05	1.2247E+02
8	1.8554E+00	6.2806E-02	2.1188E-01	96	3.8774E+05	1.3067E+02
9	2.3824E+00	7.3594E-02	2.5533E-01	97	4.0762E+05	1.3935E+02
10	3.0590E+00	8.4720E-02	3.0502E-01	98	4.5049E+05	1.4883E+02
11	3.9279E+00	9.7018E-02	3.6269E-01	99	4.9787E+05	1.5885E+02
12	5.0435E+00	1.0935E-01	4.3066E-01	100	5.2340E+05	1.6989E+02
13	6.4760E+00	1.2199E-01	5.1152E-01	101	5.5023E+05	1.8333E+02
14	8.3153E+00	1.3577E-01	6.0599E-01	102	5.7844E+05	1.9892E+02
15	1.0677E+01	1.5092E-01	7.1741E-01	103	6.0810E+05	2.1314E+02
16	1.3710E+01	1.6653E-01	8.5057E-01	104	6.3928E+05	2.2724E+02
17	1.7603E+01	1.8328E-01	1.0087E+00	105	6.7206E+05	2.4405E+02
18	2.2603E+01	2.0132E-01	1.2057E+00	106	7.0651E+05	2.6246E+02
19	2.9023E+01	2.2049E-01	1.4445E+00	107	7.4274E+05	2.8202E+02
20	3.7267E+01	2.4096E-01	1.7241E+00	108	7.8082E+05	3.0468E+02
21	4.7851E+01	2.6320E-01	2.0860E+00	109	8.2085E+05	3.2987E+02
22	6.1442E+01	2.8679E-01	2.5212E+00	110	8.6294E+05	3.7235E+02
23	7.8893E+01	3.1196E-01	3.0622E+00	111	9.0718E+05	4.0976E+02
24	1.0130E+02	3.3812E-01	3.7190E+00	112	9.6164E+05	4.4865E+02
25	1.3007E+02	3.6622E-01	4.5394E+00	113	1.0026E+06	4.9102E+02
26	1.6702E+02	3.9592E-01	5.5992E+00	114	1.1080E+06	5.3833E+02
27	2.1445E+02	4.2839E-01	7.0039E+00	115	1.1648E+06	5.9022E+02
28	2.7536E+02	4.6334E-01	8.8197E+00	116	1.2246E+06	6.4878E+02
29	3.5358E+02	5.0184E-01	1.1376E+01	117	1.2873E+06	7.1355E+02
30	4.5400E+02	5.4134E-01	1.4812E+01	118	1.3534E+06	7.8717E+02
31	5.8295E+02	5.8203E-01	1.8194E+01	119	1.4227E+06	8.6802E+02
32	7.4852E+02	6.3113E-01	2.2087E+01	120	1.4957E+06	9.5799E+02
33	9.6112E+02	6.7730E-01	2.9386E+01	121	1.5724E+06	1.0684E+03
34	1.2341E+03	7.3090E-01	4.0376E+01	122	1.6530E+06	1.1983E+03
35	1.5846E+03	7.8609E-01	5.6892E+01	123	1.7377E+06	1.3303E+03
36	2.0347E+03	8.4649E-01	6.7284E+01	124	1.8268E+06	1.4782E+03
37	2.2487E+03	9.1588E-01	7.7404E+01	125	1.9205E+06	1.6415E+03
38	2.4852E+03	9.8811E-01	8.9898E+01	126	2.0190E+06	1.8374E+03
39	2.6126E+03	1.0680E+00	1.0461E+02	127	2.1225E+06	2.1337E+03
40	2.7465E+03	1.1565E+00	1.2208E+02	128	2.2313E+06	2.4503E+03
41	3.0354E+03	1.2519E+00	1.4299E+02	129	2.3069E+06	2.9574E+03
42	3.3546E+03	1.3678E+00	1.6800E+02	130	2.3457E+06	3.5151E+03
43	3.7074E+03	1.4921E+00	1.9770E+02	131	2.3653E+06	4.0631E+03
44	4.3074E+03	1.6125E+00	2.3310E+02	132	2.3852E+06	4.9626E+03
45	5.5308E+03	1.7451E+00	2.7712E+02	133	2.4660E+06	5.8247E+03
46	7.1017E+03	1.8909E+00	3.3474E+02	134	2.5924E+06	7.4219E+03
47	9.1188E+03	2.0539E+00	4.3998E+02	135	2.7253E+06	1.0478E+04
48	1.0595E+04	2.2237E+00	5.5215E+02	136	2.8650E+06	1.3517E+04
49	1.1709E+04	2.4126E+00	6.9877E+02	137	3.0119E+06	1.8046E+04
50	1.5034E+04	2.6141E+00	8.8991E+02	138	3.1664E+06	2.3172E+04
51	1.9305E+04	2.8261E+00	1.1338E+03	139	3.3287E+06	2.6462E+04
52	2.1875E+04	3.0639E+00	1.4851E+03	140	3.6788E+06	2.8876E+04
53	2.3579E+04	3.3170E+00	1.9844E+03	141	4.0657E+06	4.1369E+04
54	2.4176E+04	3.5782E+00	2.9326E+03	142	4.4933E+06	8.6949E+04
55	2.4788E+04	3.8647E+00	4.4149E+03	143	4.7237E+06	1.3271E+05
56	2.6058E+04	4.3572E+00	6.9022E+03	144	4.9659E+06	1.4364E+05
57	2.7000E+04	4.6320E+00	1.2760E+04	145	5.2205E+06	1.6016E+05
58	2.8500E+04	4.9771E+00	2.5729E+04	146	5.4881E+06	1.8268E+05
59	3.1828E+04	5.3663E+00	8.3906E+04	147	5.7695E+06	1.8910E+05
60	3.4307E+04	5.8191E+00	1.9535E+05	148	6.0653E+06	1.9964E+05
61	4.0868E+04	6.5011E+00	2.4511E+05	149	6.3763E+06	2.1186E+05
62	4.6309E+04	6.9427E+00	2.8803E+05	150	6.5924E+06	2.2381E+05
63	5.2475E+04	7.5697E+00	4.5997E+05	151	6.7032E+06	2.5150E+05
64	5.6562E+04	8.1488E+00	1.5131E+06	152	7.0469E+06	2.6505E+05
65	6.7379E+04	9.0600E+00	2.9021E+06	153	7.4082E+06	2.7955E+05
66	7.2000E+04	9.8914E+00	5.1191E+06	154	7.7880E+06	2.9050E+05
67	7.9500E+04	1.1139E+01	8.4061E+06	155	8.1873E+06	3.0122E+05
68	8.2500E+04	1.2527E+01	1.2839E+07	156	8.6071E+06	3.2028E+05
69	8.6517E+04	1.3858E+01	1.9640E+07	157	9.0484E+06	3.3839E+05
70	9.8037E+04	1.5251E+01		158	9.5123E+06	3.8740E+05
71	1.1109E+05	1.6708E+01		159	1.0000E+07	4.6861E+05
72	1.1679E+05	1.8030E+01		160	1.0513E+07	6.0368E+05
73	1.2277E+05	1.8704E+01		161	1.1052E+07	6.9169E+05
74	1.2907E+05	1.9274E+01		162	1.1618E+07	1.4772E+06
75	1.3569E+05	2.1584E+01		163	1.2214E+07	2.3499E+06
76	1.4264E+05	2.3863E+01		164	1.2523E+07	2.7826E+06
77	1.4996E+05	2.7663E+01		165	1.2840E+07	3.2254E+06
78	1.5764E+05	3.1341E+01		166	1.3499E+07	4.1000E+06
79	1.6573E+05	3.5268E+01		167	1.3840E+07	5.2725E+06
80	1.7422E+05	3.9728E+01		168	1.4191E+07	5.9859E+06
81	1.8316E+05	4.6974E+01		169	1.4550E+07	7.8217E+06
82	1.9255E+05	5.2774E+01		170	1.4918E+07	9.9952E+06
83	2.0242E+05	6.0563E+01		171	1.5683E+07	1.1994E+07
84	2.1280E+05	6.4096E+01		172	1.6487E+07	1.3138E+07
85	2.2371E+05	6.7702E+01		173	1.6905E+07	1.3840E+07
86	2.3518E+05	7.1574E+01		174	1.7333E+07	1.4129E+07
87	2.4724E+05	7.5645E+01		175	1.9640E+07	1.9640E+07